ADVANCED MATERIALS
www.advmat.de

Toward Chiral Lasing from All-Solution-Processed Flexible Perovskite-Nanocrystal–Liquid-Crystal Membranes

Weixi Lin, Chao Yang, Yu Miao, Sen Li, Limin Zhang, Xiao-Fang Jiang, Ying Lv, Bed Poudel, Kai Wang,* Lakshminarayana Polavarapu,* Chen Zhang, Guofu Zhou,* and Xiaowen Hu**

Circularly polarized (CP) coherent light sources are of great potential for various advanced optical applications spanning displays/imaging to data processing/encryption and quantum communication. Here, the first demonstration of CP amplified spontaneous emission (ASE)/lasing from a free-standing and flexible membrane device is reported. The membrane device consists of perovskite nanocrystals (PNCs) and cholesteric liquid crystals (CLCs) layers sandwiched within a Fabry–Pérot (F–P) cavity architecture. The chiral liquid crystal cavity enables the generation of CP light from the device. The device is completely solution-processable and displays CP ASE with record dissymmetry factor (g_{lum}) as high as 1.4, which is 3 orders of magnitude higher as compared with g_{lum} of CP luminescence of chiral ligand-capped colloidal PNCs. The device exhibits ultraflexibility as the ASE intensity remains unchanged after repeated 100 bending cycles and it is stable for more than 3 months with 80% of its original intensity. Furthermore, the ultraflexibility enables the generation of ASE from various objects of different geometric surfaces covered with the flexible perovskite membrane device. This work not only demonstrates the first CP ASE from a PNCs membrane with extremely high g_{lum} but also opens the door toward the fabrication of ultraflexible, extremely stable, and all solution-processable perovskite chiral laser devices.

1. Introduction

Circularly polarized (CP) photons with intrinsically associated spin angular momentum play a crucial role in both classical and quantum optics and have already shown immense potential in many fields of science and technology including advanced spectroscopy,[1] 3D displays,[2] holographic imaging,[3] optical communication,[4] memory and logic operations, anti-counterfeiting, and data encryption.[5] The interaction of optical spin with materials has led to various intriguing phenomena as well as many state-of-the-art applications covered by the emerging scientific domains such as chiroptoelectronics, ferroelectrics, and spin photonics.[6] However, the fabrication of an advanced and high-performance flexible-material platform that generates CP lasing (also, spontaneous CP light) with high quantum efficiency and high dissymmetry factor ($g_{lum} = 2[I_L - I_R]/[I_L + I_R]$, where I_L and I_R are the intensities of left- and

W. Lin, C. Yang, Y. Miao, S. Li, L. Zhang, G. Zhou, X. Hu
SCNU-TUE Joint Lab of Device Integrated Responsive Materials (DIRM)
National Center for International Research on Green Optoelectronics
South China Academy of Advanced Optoelectronics
South China Normal University
Guangzhou 510006, P. R. China
E-mail: guofu.zhou@m.scnu.edu.cn; xwhu@m.scnu.edu.cn

W. Lin, C. Zhang
Peng Cheng Laboratory (PCL)
Shenzhen 518055, P. R. China

Y. Miao, X.-F. Jiang
Guangdong Provincial Key Laboratory of Quantum Engineering and Quantum Materials
School of Physics
South China Normal University
510006 Guangzhou, P. R. China
E-mail: jiangxf@scnu.edu.cn

Y. Lv
State Key Laboratory of Luminescence and Applications
Changchun Institute of Optics
Fine Mechanics and Physics
Chinese Academy of Sciences
Changchun 130033, P. R. China

B. Poudel, K. Wang
Material Research Institute
Pennsylvania State University
University Park, PA 16802, USA
E-mail: kaiwang@psu.edu

L. Polavarapu
CINBIO
Universidad de Vigo
Materials Chemistry and Physics Group
Department of Physical Chemistry
Campus Universitario Lagoas Marcosende
Vigo 36310, Spain
E-mail: L.Polavarapu@physik.uni-muenchen.de

The ORCID identification number(s) for the author(s) of this article can be found under https://doi.org/10.1002/adma.202301573

DOI: 10.1002/adma.202301573

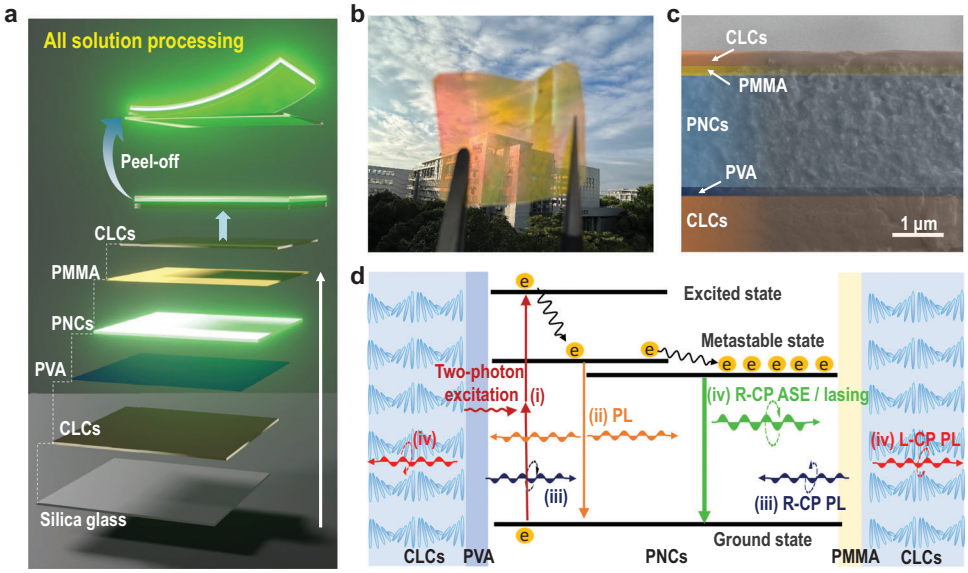

Figure 1. Processing and mechanism of the CP lasing membrane. a) Schematic of the ASE device fabricated by full-solution processing. b) Photograph of the as-prepared free-standing membrane that exhibits ASE. c) Cross-sectional SEM image of an exemplified device. d) The working mechanism of the CP ASE/lasing. The two CLC layers selectively reflect right-handed light and the light gets amplified and eventually leading to polarization selectivity.

right-handed CP emission, respectively) is extremely challenging.[7] Although the CP light (CPL) can be generated from unpolarized light using a combination of a linear polarizer with quarter-wave plate, it suffers from energy loss, rigidity and complex device setup that is difficult to be integrated with miniaturized devices. Alternatively, luminescent materials with chiral symmetry can directly emit CPL without the use of optical components.[7,8] Over the years both inorganic semiconductor and organic molecular (dyes and polymers) emitters have been exploited as sources for CPL.[9] Recently, metal halide perovskites have emerged as excellent emitters with interesting optoelectronic properties.[10] Particularly, colloidal lead halide PNCs have been generating a great deal of excitement in the laser research community owing to their high photoluminescence quantum yield (PLQY) (close to unity for Br and I-based PNCs),[11] low defect densities (defect tolerance)[12] and high radiative recombination efficiencies,[10a,13] which makes them excellent candidates for lasing and other light emitting applications.[13b,14] In order to induce chirality in colloidal perovskites so that they emit CPL, prior attempts such as modifying PNCs surface with chiral ligands, or by self-assembly into helices using nano-helical templates have been demonstrated.[15] However the g_{lum} for chiral ligand capped PNCs is only in the range of 10^{-4} to 10^{-3},[15h,16] while the chiral assemblies exhibit slightly higher g_{lum} (up to 0.1–0.2).[15c,g,h] Recently, a few studies have demonstrated the generation high g_{lum} (in the range of 1.1–1.9) CPL from halide PNCs by coupling their emission with cholesteric liquid crystals (CLCs) having periodic helical structure that triggers the optical selectively Bragg reflection.[17] These important milestones have proven the potentiality of PNCs–CLCs architectures to generate efficient CPL with high g_{lum}. Despite continuous progress in PNCs-based chiral emitters, CP lasing from such systems is yet to be realized especially from flexible devices.

Herein, we report the first demonstration of CP amplified spontaneous emission (ASE) from a free-standing and flexible membrane device consisting of PNCs and CLCs layers sandwiched within a Fabry–Pérot (F–P) cavity architecture. The CLCs layer induces the chiral emission in the device through selectively Bragg reflection and the CPL get amplified by the F–P resonator at low excitation threshold (2.4 μJ cm^{-2}). The device is completely solution processable and ultraflexible, and exhibit CP ASE with g_{lum} as high as 1.4. The device retains its ASE intensity even after 100 bending cycles and it is stable for over 3 months. Furthermore, we have demonstrated the generation of ASE from various objects with bumpy surfaces that are covered with the flexible perovskite CP ASE device.

2. Results and Discussion

First, we developed an all-solution process to fabricate the free-standing and flexible PNCs–CLCs membrane following layer by layer (CLCs/poly(vinyl alcohol) (PVA)/PNCs/poly(methyl methacrylate) (PMMA)/CLCs) deposition and peel-off process (See Experimental Section in Supporting Information for details). The device architecture is illustrated in **Figure 1**a, it was fabricated by layer-by-layer solution coating on a solid support substrate, which can be easily detached from the deposited layers by a peel-off process. In principle any substrate that is compatible for the peel-off process can be used for the fabrication of the free-standing laser device, here we randomly chosen silica glass as the support substrate. In the layer-by-layer fabrication process (Figure 1a), CLCs mixture was first blade-coated on top of the silica glass, followed by polymerization into a film under UV irradiation and then PVA solution dissolved in deionized water was spin-coated onto the surface of CLCs film. Next, PNCs dispersion was drop-casted onto the PVA layer to obtain a PNCs film, which was then covered with another spacer layer of PMMA

by spin-coating. Lastly, a layer of CLCs was deposited on top of PMMA by blade coating and then the support substrate was detached to obtain free-standing and flexible laser device. The PVA and PMMA are optical spacer layers that controls the distance between the two CLCs layers of the device to attain an F–P resonant cavity. Previously, transparent metal oxide films (e.g., Al_2O_3) or metal halide (e.g., LiF) has been used as a spacer layer to build the optical cavity, but remains cumbersome in manufacturing considering their high cost and requirement sophisticated deposition techniques such as atomic layer deposition,[18] magnetron sputtering,[19] or other high vacuum and high temperature processing (>600 °C).[20] Here, both the PVA and PMMA layer are fabricated by solution processed and annealed at low temperature (60 °C). Meanwhile, the PVA layer can protect the CLCs layer from erosion by the subsequent deposition of PNCs layer using the colloidal nanocrystals (NCs) dispersed in toluene, and also enhance the quantum efficiency of the PNCs layer through surface passivation (Figures S1 and S2, Supporting Information). On the other hand, the PMMA layer make the PNCs film much smoother (Figure S3, Supporting Information) while protecting it against the erosion from the xylene used to dissolve CLCs, and thus help to obtain a better CLCs reflector with less roughness and higher reflection.

The photograph of the device is shown in Figure 1b. The device is highly flexible and semitransparent. The cross-sectional scanning electron microscopy (SEM) image of the fabricated ASE device is shown Figure 1c. The thickness of the resonant medium (PVA/PNCs/PMMA) in the device is set to 2.7 μm to match with an F–P resonator cavity characteristic dimensions, i.e., 10/(2×270 nm) ($10/2\lambda$).[18,20] The thickness of the top CLCs layer is controlled to ≈500 nm, which is thinner than that of the bottom CLCs layer (≈1.5 μm), in order to have a lower reflectivity from one of the facets for the ASE/lasing output. The CLCs films with right handedness as both top and bottom reflectors were used to selectively reflect right-handed CPL and eventually leading to polarization selectivity. The working mechanism of the device is illustrated in Figure 1d. Briefly, the PNCs are excited with an 800 nm fs pulse laser based on two-photon absorption (i). The excited state electrons can decay either toward the metastable state or to the ground state through spontaneous emission (ii). When the excitation intensity is large enough to produce population inversion, which then leads to ASE in PNCs. As the PNCs film is sandwiched between two right-handed CLCs reflectors, only the right-handed CP (R-CP) emission can be reflected (iii) constantly in the cavity and amplified, while the left-handed CP (L-CP) emission transmit outward (iv), which eventually leads to a strong output of R-CP ASE/Lasing emission (v).

To demonstrate CP lasing using the above-discussed device, we have chosen $CsPbBr_3$ NCs as the gain medium owing to their near-unity PLQY and bright green emission (visible and relatively easy to probe during the experiment). The $CsPbBr_3$ NCs were synthesized by modified hot-injection method (see the Experimental Section in Supporting Information for details).[21] **Figure 2**a shows the transmission election microscopy (TEM) image of the as-synthesized $CsPbBr_3$ NCs, showing typical cubic morphology with a narrow size distribution of 10.1 ± 0.5 nm (see large-area TEM in Figure S4, Supporting Information). Figure 2b shows the SEM images of the surface of the PNCs film obtained by drop-casting, it displays uniform and continuous features without significant voids. The cross-sectional image (inset of Figure 2b) quantifies the film thickness of 1.5 μm. The PNCs film was further characterized by UV–vis and PL spectroscopy. As shown in Figure 2c, the PNCs film exhibits a PL peak at 525 nm with a narrow linewidth of 20 nm (88 meV) and is Stokes-shifted by 25 nm (109 meV) with respect to the excitonic absorption peak located at ≈500 nm. Power dependent PL spectra of the PNCs film was obtained under two-photon pump excitation at 800 nm with 100 fs pulse (Figure 2d). At a low excitation power (<10 μJ cm^{-2}), the film emits typical PL with a single-peak spectrum centered at a wavelength of ≈525 nm. When the excitation power exceeds a threshold of 12.4 μJ cm^{-2}, an ASE appears with a secondary emission peak at 540 nm, which is red-shifted by 15 nm with respect to the PL maximum. The second peak exhibits a narrower bandwidth with a full-width at half maximum (FWHM) of 5 nm, typical evidence for ASE/lasing (Figure 2e).

To investigate the CPL from the PNCs–CLCs films, the polarization state of the emission is analyzed using L-CP and R-CP filters consist of a $\lambda/4$ waveplate and a polarizer in front of the optical fiber that is used for the collection of light (see schematic illustration of the setup in Figure 2g). The real actual optical setup used for the CPL measurements is shown in Figure S5 (Supporting Information). Thus, the acquired CPL spectra of the PNCs film under the excitation power density of 15 μJ cm^{-2} is depicted in Figure 2f. It is found that the L- and R- CP light (ASE) from the PNCs film show identical emission spectra with same intensity. Chirality is often quantified with g_{lum}, which can be maximum 2 for ideal chiral photonic structures. A positive g_{lum} indicates the left-handed circularly polarization of the output radiation, while a negative g_{lum} suggest the right-handed circularly polarization.[22] Here the pristine PNCs film display a g_{lum} value of 0 because of the same intensity of L- and R- CP light, suggesting the none circularly polarization nature of the PNCs film.

To induce CPL from PNCs film, a CLCs polymer film is introduced on one side of the PNCs film. The device architecture is illustrated in **Figure 3**ai, where first a right-handed CLCs film is deposited on silica substrate and then thin polymer buffer layer of PVA is used as an optical spacer layer before introducing the PNCs layer. Because of the selective reflection by the right-handed CLCs film, L-CP light of the PNCs emission can transmit through the stacks, while the R-CP light of the emission with the wavelength located inside the photonic bandgap (PBG) of the CLCs film is reflected. Therefore, the intensities of L-CP and R-CP light are different in both side of the stacks, and thus leading to CPL with non-zero g_{lum}. Figure 3aii shows the molecular structure of the materials used for preparing the CLCs mixture, the materials that is inspired from our previous report (see Experimental Section in Supporting Information for details of making CLCs mixture and the film). Here, RM-257 is a diacrylate monomer, which can be cross-linked into a polymer network under UV irradiation with the assistance of the photo-initiator of Irgacure-651. A surfactant is used to control the liquid crystal alignment at the air interface and to avoid de-wetting during the coating process. LC-756 is a chiral monomer, which gives a helix with a right-handed rotation and consequently, enabling the CLCs film to reflect right-handed CPL. The wavelength of the light that can be reflected by the CLCs layer, is calculated as $\Delta\lambda = \Delta n \times p = (n_e - n_o) \times p$, where Δn is the birefringence index of the CLC mixture, and n_e and n_o are the extraordinary

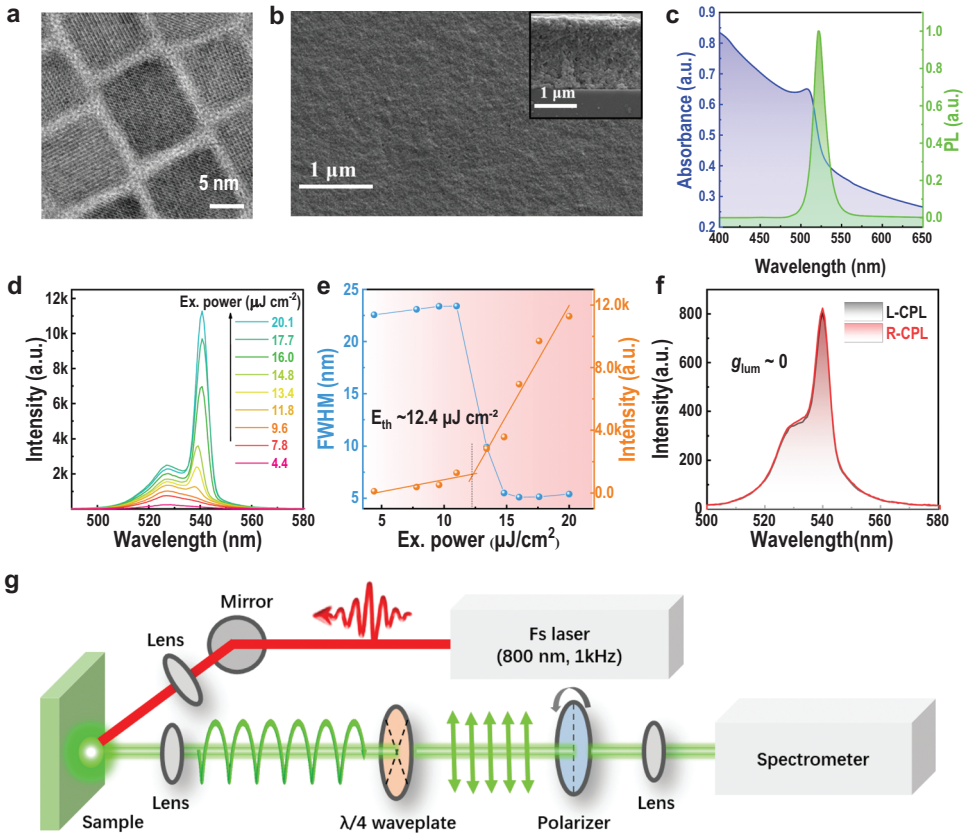

Figure 2. Characterization of the PNCs film. a) TEM image of the as-synthesized $CsPbBr_3$ NCs. b) SEM image of the surface of the PNCs film. c) Optical absorption and PL spectra of the PNCs film. d) Power dependence of the emission spectra from the PNCs film. e) Pump-dependent PL intensity and FWHM of the PNCs film. f) The measured CPL spectra of the PNCs film probed with a L- and R-CP polarizer under the excitation power of 15 μJ cm^{-2}. The PNCs film is excited at $\lambda = 800$ nm with 100 fs laser pulses. g) Schematic illustration of the optical setup for characterization of CPL.

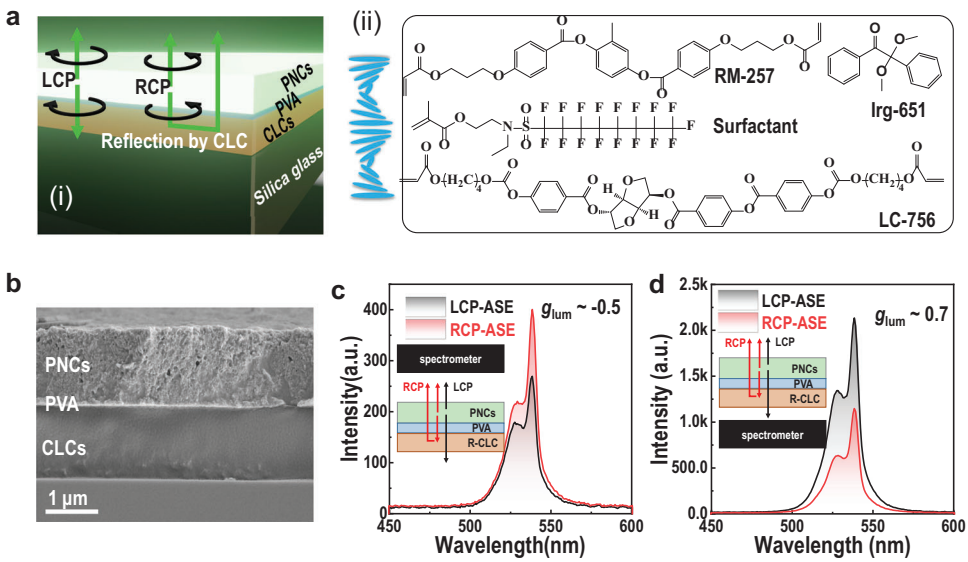

Figure 3. Characterization of the CPL properties of a CLCs/PVA/PNCs stack. a) i) Scheme of a composite stack with a structure of CLCs/PVA/PNCs. ii) The structure of the molecules used in making CLCs films. b) SEM cross-section image of the CLCs/PVA/PNCs composite stack. c,d) CPL spectra of the composite stack measured from PNCs side (c), and from CLCs side (d) under the excitation power of 7 μJ cm^{-2}. The inset shows the detection direction of CPL.

and ordinary refractive indexes, respectively, and p is the helical pitch of the CLCs film, which is defined by equation of $p = 1/(\mathrm{HTP} \times c)$ where HTP is the helical twisting power of the chiral monomer and c is the concentration of the chiral monomer in the CLC mixture.[23] By adjusting the concentration of LC-756 in the CLCs mixture, the reflection band of CLCs film is controlled to be centered at 540 nm, so that it matches the peak of ASE (540 nm) spectra of the PNCs film, but allowing sufficient transmission of the excitation beam (i.e., 800 nm). We then quantified the spectral reflection/transmittance feature of the CLCs film (Figure S6, Supporting Information). The transmittance of L-CP light is nearly 100% (red line, suggesting fully transparent for the L-CP Light) in the wavelength range of 450 to 700 nm, while the transmittance of R-CP light is ≈10% at the same conditions (suggests ≈90% R-CP light is reflected by the CLCs film). Thus, the CLCs layer selectivity transforms the emission of the PNCs film into CPL by selective reflection of right CP part of the emission. Figure 3b shows the cross-sectional SEM image of the fabricated layer stack, the CLCs layer is well protected by the multifunctional PVA layer and isolated from the PNCs film, as evidenced by the identical thickness of 1.5 µm.

We further characterize the optical properties of the device by two-photon PL measurement with different excitation intensities. As the pump-power increases, ASE peak centered at a wavelength of 540 nm appears from the composite film at a threshold of 5.6 µJ cm^{-2} (Figure S7a and S7b, the threshold is smaller compared to the PNCs layer without CLCs, as depicted in Figure 2e). There are likely two reasons for the reduction of ASE threshold. One is due to the PL enhancement of the PNCs by the PVA layer[24] and the other is the reflection of light by CLCs layer. The CLCs reflector layer can redirect the emission to propagate along both the out-of-plane cavity, and oblique paths back into the PNCs film, leading to an increased optical path length in the active layer, which results in a low lasing threshold.[18,20] We then studied the polarization (L-or R-) of the ASE resulting from CLCs layer by collecting the emission either on the PNCs layer side or the CLCs layer side, as illustrated in the insets of Figure 3c,d. When the detector is positioned at the front side of PNCs layer (inset of Figure 3c), the intensity of R-CP ASE is 1.5-fold higher than that of the L-CP ASE, leading to a g_{lum} of −0.5 at a wavelength of 540 nm (Figure 3c). In contrast, when the detector is positioned at the CLC facet side (inset of Figure 3d), the L-CP ASE is 1.9-fold higher than that of R-CP ASE, resulting a $g_{lum}$of +0.7 (Figure 3d). Furthermore, the wavelength dependence of g_{lum} for both the cases is further calculated and depicted in Figure S7c and S7d, respectively. Notably, the sign of g_{lum} reversed by changing the detector from one side to the other, suggesting that the device generate reversed CPL from the opposite sides of the stack films. This asymmetric polarized emission can be ascribed to the selective reflection of the CLCs film, where the major portion of the R-CP light from PNCs can be sufficiently reflected backward to the PNCs layer and further emit from that surface with higher intensity (Figure 3c). On the other hand, the CLCs layer allows L-CP light to pass through but reflects R-CP light and consequently resulting in L-CP emission from the CLCs side (Figure 3d).

These promising results show that the laminar stacking of CLCs/PVA/PNCs layers can generate CP ASE from both sides of the device. To further enhance the lasing performance and invoke the selectivity of L-CP and R-CP emission, we built a resonate cavity by depositing another CLCs reflector on top of PNCs layer but using a PMMA spacer. **Figure 4**a illustrate the sandwich device with a structure made of CLCs/PVA/PNCs/PMMA/CLCs layers, and the SEM of the real device can be seen in Figure 1c. The PL properties of the device is studied under two-photon excitation by collecting the emission from the front side of top CLCs, as indicated in Figure 4a. As the excitation power increases the PL peak at 525 nm turns into ASE peak at 540 nm (Figure 4b) and is like the PL characteristics of the CLCs/PVA/PNCs device. Power-dependent PL intensity and FWHM of the device is depicted in Figure 4c, which show that the device exhibits a small lasing threshold of 2.4 µJ cm^{-2}. Such a low lasing threshold can be ascribed to the CLCs-based F–P cavity. The CLCs reflectors can redirect the emission propagating along the out-of-plane cavities, which leads to an enhanced optical path length in the medium and enhances the wave-guiding capability of the PNCs film, resulting in a low ASE/lasing threshold.[25]When the pump intensity exceeds the lasing threshold, the FWHM of the emission is reduced from 20 to 4 nm. However, the FWHM of 4 nm is still higher than that typically observed for lasing. As the CLCs cavity is wide, one would expect multimode lasing. The ASE-like emission is likely due to the low resolution of the detector that cannot resolve ultranarrow lasing peaks. When using a high-resolution spectrometer with a wavelength resolution of 0.05 nm, multimode lasing can be clearly seen (Figure S8, Supporting Information). Our future studies will be focused on the optimization of the CLCs cavity to realize single mode chiral lasing using high-sensitivity detector. To further verify characteristics of the multimode lasing, we perform numerical simulations to understand the multi-resonant frequencies in the device (see Figure S9, Supporting Information). The refractive index and extinction coefficients used in the numerical simulations are obtained from ellipsometry measurements (Figure S10, Supporting Information). We simulated the wavelength (frequency)-dependent electric field strength distribution throughout the device. It is observed that the eigenfrequencies of 552.89, 553.18, 557.89, 558.36, and 560.53 THz are compatible with the resonant cavity of the device to trigger the lasing effect. The resonant frequencies from 552.89 to 560,53 THz are corresponding to different lasing wavelengths from 535 to 543 nm. Thus, the multimode lasing can be ascribing to the overlap of these different emission peaks.

We then investigate the excitation-dependent CPL properties of the sandwich device under two photon excitations. At low pump intensity (e.g., 2.0 µJ cm^{-2}), the device emits 18% higher L-CP light than R-CP light (Figure 4d) with a positive g_{lum} of 0.24. In contrast, at high pump intensity (e.g., 3.7 µJ cm^{-2}), the intensity of R-CP lasing is remarkably higher (82%) than that of L-CP lasing (Figure 4e) with a g_{lum} of −1.4. Despite the first report on PNCs based CP lasing/ASE, this is one of the highest g_{lum} ever reported for CPL of PNCs based materials (Table S3, Supporting Information). Figure 4f shows the optical activity g_{lum}spectra of the device excited at the power energy of 3.7 µJ cm^{-2}. The insets in Figure 4f show the corresponding photographs of the emission from the sandwich device filtered by a right-handed or a left-handed circular polarizer. There is an obvious higher brightness from the device photographed through a right-handed polarizer, implying to strong R-CP lasing. The CP characteristics of the lasing emission is further corroborated by recording the

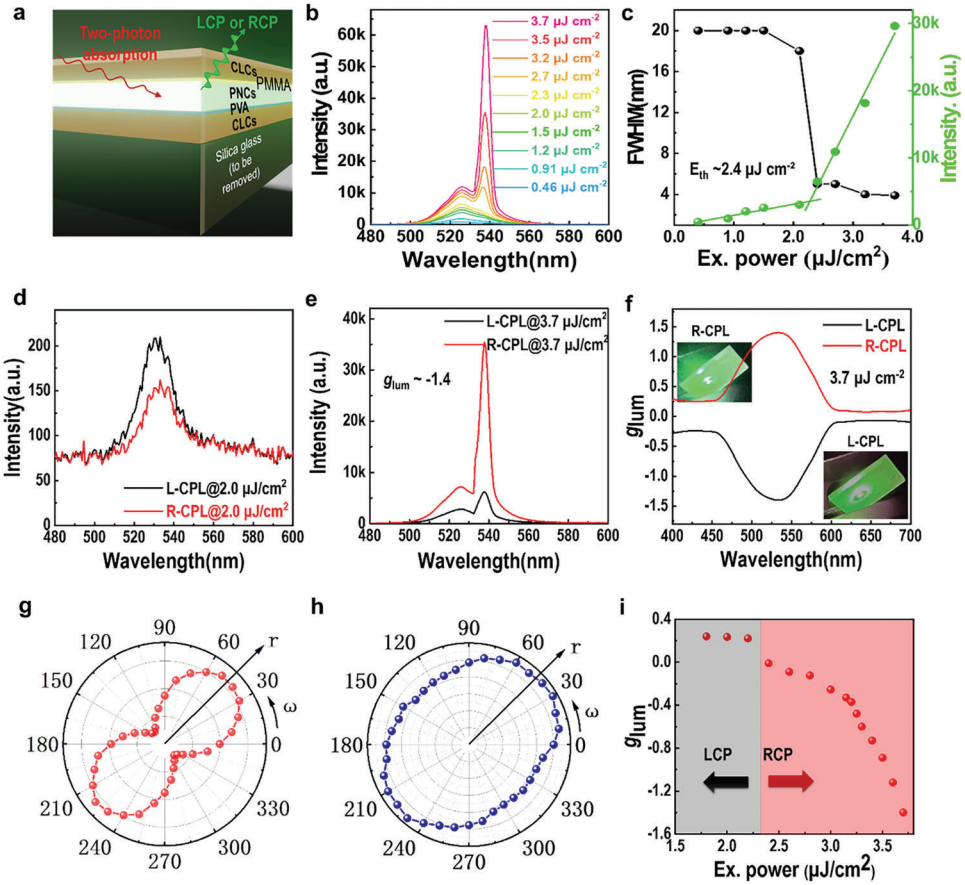

Figure 4. Characterization of the CP lasing. a) Schematic showing the structure of PNCs–CLCs laser device. b) Evolution of PL spectra of the device with the increase in excitation power. c) Pump-dependent PL intensity and FWHM of the PNCs–CLCs laser device. d) The measured CPL spectra of the device under the excitation power of 2 μJ cm^{-2}. e) The measured CPL spectra of the device under the excitation power of 3.7 μJ cm^{-2}. f) g_{lum} spectra of L- and R-CPL under the excitation power of 3.7 μJ cm^{-2}. The insets show the pictures of the device through a left- and right-handed polarizer. g,h) Emission intensity of right-handed CP lasing as a function of polarization angle with and without a quarter wavelength plate in the polar coordinate system, where the polar angle ω is the transmission angle of the polarizer, and the radius r is the transmittance. i) Evolution for the dissymmetric factor of the device with the increase in pump energy.

transmittance of the light passing through a $\lambda/4$ waveplate followed by a rotated analyzer. The $\lambda/4$ waveplate converts CPL to linear polarized light that can be readily examined by a linear analyzer. As shown in Figure 4g, the R-CP lasing is converted into a linear polarized light with orthogonal plane polarization. However, upon removing the $\lambda/4$ waveplate, the shape of the graph is elliptical instead of a perfect circle due to the small percentage of L-CPL in the emission (Figure 4h). The oval shape distribution of the R-CPL intensity indicates that the dissymmetry factor ($|g_{lum}|$) of the CP lasing is less than 2, which is in consistence with the $|g_{lum}|$ of 1.4 obtained. We further measured the L-CP and R-CP light spectra under different pump energies using circular polarizer and depicted in Figure S11 (Supporting Information). Figure 4i shows the pump-power dependent g_{lum} of CPL and it is tunable from +0.24 to −1.4 with pump intensity varied from 2.0 to 3.7 μJ cm^{-2}.

The excitation-intensity-dependent reversibility of the sign (+ or −) of g_{lum} can be understood by the synergistic effect of ASE and CLCs reflection. First, the two-photon excitation of PNCs generates equivalent L-CP and R-CP emission where the R-CP emission is mostly reflected by the two CLCs layers and confined within the sandwich structure. As illustrated in Figure S12 (Supporting Information), at low pump intensity, L-CP light can freely pass through the CLCs layer and emit outwards while the R-CP is confined within the device. Thus, the intensity of L-CP light detected is higher than that of R-CP light, resulting in a positive g_{lum}. In contrast, at high pump intensity exceeding the threshold, R-CP emission that is reflected into the cavity will trigger the ASE/lasing effect in the cavity. This significantly magnifies the intensity and eventually lead to a strong R-CP ASE/lasing. Despite the small portion of L-CP light, the g_{lum} of −1.4 is listed as a high value for CP ASE/lasing.[18,20]

According to the reflectivity of a CLCs layer, at high pump intensity, the L-CP spontaneous emission is supposed to be higher than that of R-CP spontaneous emission. However, in Figure 4e, we observed that the intensity of R-CP spontaneous emission is higher than that of L-CP spontaneous emission, which is like the case of the ASE peak. This is because the transmittance spectra of the CLCs layer for L- and R-polarized light span from ≈480–570 nm with a peak maximum at ≈540 nm, and it is in resonant

with the emission spectra (both the spontaneous and amplified spontaneous) of PNCs film (Figure S6, Supporting Information). We explain this inconsistency as follows. The CLCs layers act as a 1D photonic crystals (PCs) that exhibits a PBG characteristics through a selective Bragg reflection.[26] It is well known that PCs exhibit remarkable optical properties due to the excitation of resonant guided modes by the incident light, which results in a significant enhancement of the electromagnetic fields at the surface of PCs.[27] Here, the PBG of the CLCs layer spans from ≈480–570 nm, which covers the wavelength of both the spontaneous emission (525 nm) and ASE (540 nm) of PNCs film. Therefore, when the PNCs is sandwiched between two right-handed CLCs layers, R-CP emission of PNCs was localized in the distributed feedback cavity. The fluorescence-resonance mode occurs at the interface of CLCs PCs and give rise to a local field enhancement of R-CP emission. This enhancement was confirmed by the nonlinearly increased intensity of R-CP spontaneous emission and ASE (see Figure S13, Supporting Information). At low excitation intensity, the R-CP spontaneous emission is suppressed by the reflection bandgap. As the excitation intensity increases, both R-CP spontaneous emission and ASE were enhanced compared to L-CP emission. To confirm the local electric field enhanced emission, we compared the emission lifetimes of PNCs (PVA/PNCs) and PNCs–CLCs (CLCs/PVA/PNCs/PMMA/CLCs) films. As shown in Figure S14 (Supporting Information), the time-resolved emission decays are biexponential for both the films. The average decay time for PNCs–CLCs film is 2.08 ns, which is shorter than that of PNCs film (3.17 ns). The shortened lifetime of spontaneous emission suggests an increased radiative decay rate, which supports the local electric field enhanced emission.[28] Although there are enhancements in both the R-CP spontaneous emission and ASE, the increase in the intensity of ASE is much higher than that of spontaneous emission, which is because ASE with highly directional photons causes higher gain in the CLCs resonant cavity.

For perovskite-based devices, achieving long-term stability is one of the most challenging and is one of the active areas of research in the field. Interestingly, our device is extremely stable without any further encapsulation as it exhibits only a slight decrease (≈5%) in emission intensity after 3 months of storage under ambient environment at a humidity of 60% and temperature of 25 °C (**Figure 5**a). The higher stability is attributed to the protection from PVA and PMMA that isolate the PNCs from moisture and oxygen. Additionally, the device exhibits relatively high operational stability under continuous excitation of the pumped-pulse laser at ambient environment. As shown in Figure 5b, the device retains the lasing efficiency higher than 80% of the initial value after continuing excitation over 20 min. This is comparable to those state-of-the-art electrical excitation green perovskite LED device (luminescent intensity decreasing to 80% in 5–10 min).[11,29] The slight decrease of the lasing efficiency may originate from the heat accumulation caused by the continuing excitation, leading to the disturbance of the CLCs resonator that degrade the device performance.

Generally, conventional F–P resonant cavity is made of Ag or Au thin-film reflectors because of their high reflectivity and are often fabricated by magnetron sputtering or vacuum evaporation, which is not compatible with low-cost, high throughput, R2R processing. In contrast, the PNCs–CLCs device is highly flexible and free standing as well as all-solution-processable without high-temperature treatment. As shown in Figure 5c, the free-standing membrane exhibits an ASE threshold of 2.9 μJ cm^{-2}, which is close to the ASE threshold of PNC film on a glass substrate (2.4 μJ cm^{-2}). Importantly, the lasing intensity of the membrane remains same even after 100 bending (180°) cycles Figure 5d, indicating exceptional mechanical flexibility.

Light source with attributes of: i) circular polarization, ii) dynamic lasing tunability (monochromaticity, coherence, directionality, and high brightness), and iii) great mechanical flexibility, can provide substantial opportunities to design, construct, and engineer new functional light applications. As a proof of concept, we demonstrate the use of the free-standing CP lasing membrane to generate light from the surface of different objects with arbitrary surfaces. As shown in Figure 5e, the membrane can stick well on sphere, sharp corner, and bended surface and emits uniform green light under UV light (365 nm) excitation. Looking forward, we anticipate the mechanical engineering and design of functional support objects on which the CP lasing membrane can be applied. For example, photonic controlling of CP lasing from predesigned object matrix with specific geometric shape can lead to further R&D directions of augmented reality (AR) applications.

3. Conclusion

We have demonstrated high-dissymmetry (g_{lum} = 1.4) chiral/CP ASE/lasing from a free-standing perovskite-CLCs layered membrane for the first time. The membrane is highly flexible and all-solution-processable and exhibits a low ASE threshold (2.4 μJ cm^{-2}). We find that the magnitude of g_{lum} and its sign is highly dependent on the excitation power, and it is continuously tunable by the pump-power. The membrane is extremely stable under many bending cycles as it retains its original PL intensity. In addition, the membrane shows long-term stability as the perovskite layer is protected by insulting PVA and PMMA layers. The low ASE threshold and great mechanical flexibility will allow the application of the PNCs–CLCs membranes as wearable optoelectronics for 3D display, optical encoding, anti-counterfeiting, soft robotic, AR, et al. Further optimization of the F–P resonator, like the quality of PNCs film and CLCs film, will likely allow a single mode CP lasing emission with narrower FWHM. In principle, the lasing wavelength is also tunable by size and composition engineering of gain media along with suitable cavity design to match the emission wavelength. We strongly believe that the approach we demonstrate here to obtain chiral lasing is applicable to other emitter systems as well. Lastly, the fully solution processing nature secures the easiness of technical transition with convenience of mass-production feasibility with high level of cost efficiency.

Supporting Information

Supporting Information is available from the Wiley Online Library or from the author.

Acknowledgements

W.L., C.Y. and Y.M. contributed equally to this work. The authors thank the support from National Key R&D Program of China (No. 2020YFE0100200),

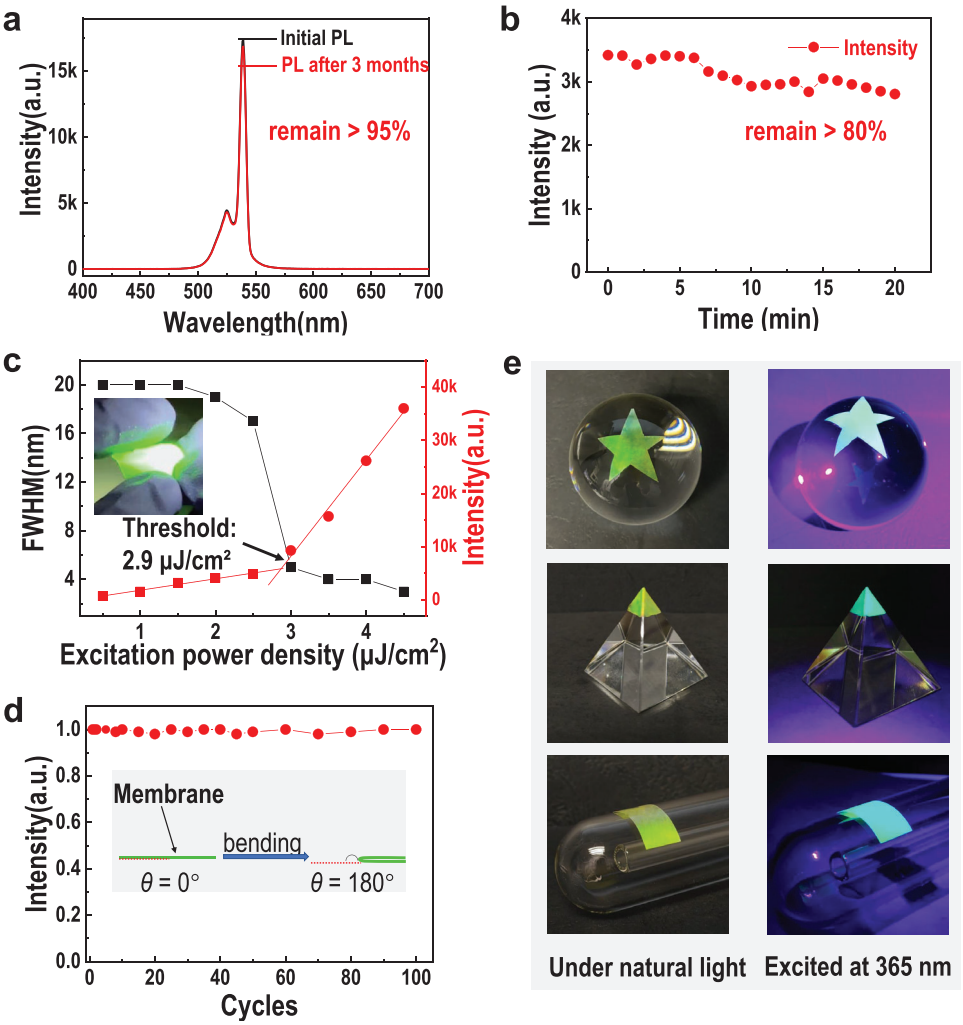

Figure 5. Stability and flexibility of the PNCs–CLCs membrane that exhibits ASE. a) Comparison of lasing intensity between the fresh device and aged device stored for three months (room temperature, ambient atmosphere with RH of ≈60%), under the same excitation power density of 3.5 μJ cm^{-2}. b) Operational stability showing the aging of the lasing intensity of the device under the continuous excitation of the pumped-pulse laser in the ambient environment. c) Pump energy density dependent PL intensity and FWHM of the PNCs–CLCs membrane lasing. The inset shows a photograph of the free-standing membrane device. d) The lasing intensity of the membrane during the repeated 180° bending cycles (100 cycles are included). e) Photographs of the ultraflexible PNCs–CLCs membranes attached on various curved surfaces with emission under UV light. ASE of flexible device under two-photon excitation is shown in Figure S15 (Supporting Information), demonstrating the device operation under flexible condition.

Natural Science Foundation of China under Grant (No. 62075065), Science and Technology Program of Guangzhou (No. 202201010344, 20202030148, 2019050001), Natural Science Foundation of Guangdong Province under Grant (No. 2021A1515010653, 2021A1515011388), the Innovation Research Project of Foshan Education Bureau under Grant (No. 2021XCL06), Guangdong Provincial Key Laboratory of Optical Information Materials and Technology (No. 2017B030301007), MOE International Laboratory for Optical Information Technologies and the 111 Project. L.P. acknowledges the support from the Spanish Ministerio de Ciencia e Innovación through the Ramón y Cajal grant (RYC2018-026103-I) and the Spanish State Research Agency (Grant No. PID2020-117371RA-I00), as well as the grant from the Xunta de Galicia (ED431F2021/05).

Conflict of Interest

The authors declare no conflict of interest.

Data Availability Statement

The data that support the findings of this study are available from the corresponding author upon reasonable request.

Keywords

circularly polarized lasing, flexible membrane, laser, liquid crystals, perovskite nanocrystals

Received: February 17, 2023
Revised: June 5, 2023
Published online: September 22, 2023

[1] J. P. Riehl, F. S. Richardson, *Chem. Rev.* **1986**, *86*, 1.

[2] X. Zhan, F. F. Xu, Z. Zhou, Y. Yan, J. Yao, Y. S. Zhao, *Adv. Mater.* **2021**, *33*, 2104418.
[3] W. Yang, S. Xiao, Q. Song, Y. Liu, Y. Wu, S. Wang, J. Yu, J. Han, D.-P. Tsai, *Nat. Commun.* **2020**, *11*, 1864.
[4] Y. Yang, R. C. Da Costa, M. J. Fuchter, A. J. Campbell, *Nat. Photonics* **2013**, *7*, 634.
[5] L. Xu, Y. Feng, D. Yu, Z. Zheng, X. Chen, W. Hong, *Adv. Mater. Technol.* **2020**, *5*, 2000373.
[6] a) R. P. Cameron, S. M. Barnett, A. M. Yao, *New J. Phys.* **2012**, *14*, 053050; b) F. Cardano, L. Marrucci, *Nat. Photonics* **2015**, *9*, 776; c) G. Long, R. Sabatini, M. I. Saidaminov, G. Lakhwani, A. Rasmita, X. Liu, E. H. Sargent, W. Gao, *Nat. Rev. Mater.* **2020**, *5*, 423; d) P. Shi, L. Du, X. Yuan, *Nanophotonics* **2021**, *10*, 3927; e) X. Zhang, Y. Liu, J. Han, Y. Kivshar, Q. Song, *Science* **2022**, *377*, 1215; f) Y. Chen, H. Deng, X. Sha, W. Chen, R. Wang, Y.-H. Chen, D. Wu, J. Chu, Y. S. Kivshar, S. Xiao, *Nature* **2023**, *613*, 474.
[7] a) G. Longhi, E. Castiglioni, J. Koshoubu, G. Mazzeo, S. Abbate, *Chirality* **2016**, *28*, 696; b) Y. Sang, J. Han, T. Zhao, P. Duan, M. Liu, *Adv. Mater.* **2020**, *32*, 1900110.
[8] Y. Deng, M. Wang, Y. Zhuang, S. Liu, W. Huang, Q. Zhao, *Light: Sci. Appl.* **2021**, *10*, 76.
[9] a) E. M. Sánchez-Carnerero, A. R. Agarrabeitia, F. Moreno, B. L. Maroto, G. Muller, M. J. Ortiz, S. de la Moya, *Chem. - Eur. J.* **2015**, *21*, 13488; b) D. Han, C. Li, C. Jiang, X. Jin, X. Wang, R. Chen, J. Cheng, P. Duan, *Aggregate* **2022**, *3*, e148; c) S. Jiang, N. A. Kotov, *Adv. Mater.* **2022**, *9*, 2108431.
[10] a) Y. Wang, X. Li, J. Song, L. Xiao, H. Zeng, H. Sun, *Adv. Mater.* **2015**, *27*, 7101; b) Q. A. Akkerman, V. D'Innocenzo, S. Accornero, A. Scarpellini, A. Petrozza, M. Prato, L. Manna, *J. Am. Chem. Soc.* **2015**, *137*, 10276; c) Y. Fu, H. Zhu, J. Chen, M. P. Hautzinger, X. Y. Zhu, S. Jin, *Nat. Rev. Mater.* **2019**, *4*, 169; d) J. Shamsi, A. S. Urban, M. Imran, L. De Trizio, L. Manna, *Chem. Rev.* **2019**, *119*, 3296; e) W. Lin, X. Hu, L. Mo, X. Jiang, X. Xing, L. Shui, S. Priya, K. Wang, G. Zhou, *Adv. Opt. Mater.* **2021**, *9*, 2100261; f) A. Dey, J. Ye, A. De, E. Debroye, S. K. Ha, E. Bladt, A. S. Kshirsagar, Z. Wang, J. Yin, Y. Wang, *ACS Nano* **2021**, *15*, 10775; g) C. Otero-Martínez, J. Ye, J. Sung, I. Pastoriza-Santos, J. Pérez-Juste, Z. Xia, A. Rao, R. L. Hoye, L. Polavarapu, *Adv. Mater.* **2022**, *34*, 2107105.
[11] Y. Dong, Y.-K. Wang, F. Yuan, A. Johnston, Y. Liu, D. Ma, M.-J. Choi, B. Chen, M. Chekini, S.-W. Baek, L. K. Sagar, J. Fan, Y. Hou, M. Wu, S. Lee, B. Sun, S. Hoogland, R. Quintero-Bermudez, H. Ebe, P. Todorovic, F. Dinic, P. Li, H. T. Kung, M. I. Saidaminov, E. Kumacheva, E. Spiecker, L.-S. Liao, O. Voznyy, Z.-H. Lu, E. H. Sargent, *Nat. Nanotechnol.* **2020**, *15*, 668.
[12] A. Fakharuddin, M. K. Gangishetty, M. Abdi-Jalebi, S.-H. Chin, A. R. bin Mohd Yusoff, D. N. Congreve, W. Tress, F. Deschler, M. Vasilopoulou, H. J. Bolink, *Nat. Electron.* **2022**, *5*, 203.
[13] a) Q. Wei, X. Li, C. Liang, Z. Zhang, J. Guo, G. Hong, G. Xing, W. Huang, *Adv. Opt. Mater.* **2019**, *7*, 1900080; b) J. Chen, W. Du, J. Shi, M. Li, Y. Wang, Q. Zhang, X. Liu, *InfoMat* **2020**, *2*, 170; c) L. Lei, Q. Dong, K. Gundogdu, F. So, *Adv. Funct. Mater.* **2021**, *31*, 2010144.
[14] a) X. Ren, X. Zhang, H. Xie, J. Cai, C. Wang, E. Chen, S. Xu, Y. Ye, J. Sun, Q. Yan, T. Guo, *Nanomaterials* **2022**, *12*, 2243; b) A. Fakharuddin, M. K. Gangishetty, M. Abdi-Jalebi, S.-H. Chin, A. R. bin Mohd Yusoff, D. N. Congreve, W. Tress, F. Deschler, M. Vasilopoulou, H. J. Bolink, *Nat. Electron.* **2022**, *5*, 203; c) Y.-H. Kim, Y. Zhai, H. Lu, X. Pan, C. Xiao, E. A. Gaulding, S. P. Harvey, J. J. Berry, Z. V. Vardeny, J. M. Luther, *Science* **2021**, *371*, 1129.
[15] a) J. Ma, H. Wang, D. Li, *Adv. Mater.* **2021**, *33*, 2008785; b) G. Long, R. Sabatini, M. I. Saidaminov, G. Lakhwani, A. Rasmita, X. Liu, E. H. Sargent, W. Gao, *Nat. Rev. Mater.* **2020**, *5*, 423; c) W. Chen, S. Zhang, M. Zhou, T. Zhao, X. Qin, X. Liu, M. Liu, P. Duan, *J. Phys. Chem. Lett.* **2019**, *10*, 3290; d) S. Jiang, Y. Song, H. Kang, B. Li, K. Yang, G. Xing, Y. Yu, S. Li, P. Zhao, T. Zhang, *ACS Appl. Mater. Interfaces* **2022**, *14*, 3385; e) Y. H. Kim, Y. Zhai, E. A. Gaulding, S. N. Habisreutinger, T. Moot, B. A. Rosales, H. Lu, A. Hazarika, R. Brunecky, L. M. Wheeler, J. J. Berry, M. C. Beard, J. M. Luther, *ACS Nano* **2020**, *14*, 8816; f) Y. H. Kim, R. Song, J. Hao, Y. Zhai, L. Yan, T. Moot, A. F. Palmstrom, R. Brunecky, W. You, J. J. Berry, J. L. Blackburn, M. C. Beard, V. Blum, J. M. Luther, *Adv. Funct. Mater.* **2022**, *32*, 2200454; g) D. Di Nuzzo, L. Cui, J. L. Greenfield, B. Zhao, R. H. Friend, S. C. J. Meskers, *ACS Nano* **2020**, *14*, 7610; h) Y. Shi, P. Duan, S. Huo, Y. Li, M. Liu, *Adv. Mater.* **2018**, *30*, 1705011; i) N. Fiuza-Maneiro, K. Sun, I. López-Fernández, S. Gómez-Graña, P. Müller-Buschbaum, L. Polavarapu, *ACS Energy Lett.* **2023**, *8*, 1152; j) J. Mendoza-Carreño, P. Molet, C. Otero-Martínez, M. I. Alonso, L. Polavarapu, A. Mihi, *Adv. Mater.* **2023**, *35*, 2210477; k) J. Ma, C. Fang, C. Chen, L. Jin, J. Wang, S. Wang, J. Tang, D. Li, *ACS Nano* **2019**, *13*, 3659.
[16] Z. N. Georgieva, B. P. Bloom, S. Ghosh, D. H. Waldeck, *Adv. Mater.* **2018**, *30*, 1800097.
[17] a) C.-T. Wang, K. Chen, P. Xu, F. Yeung, H.-S. Kwok, G. Li, *Adv. Funct. Mater.* **2019**, *29*, 1903155; b) X. Yang, M. Zhou, Y. Wang, P. Duan, *Adv. Mater.* **2020**, *32*, 2000820; c) S. Liu, X. Liu, Y. Wu, D. Zhang, Y. Wu, H. Tian, Z. Zheng, W.-H. Zhu, *Matter* **2022**, *5*, 2319.
[18] S. D. Stranks, S. M. Wood, K. Wojciechowski, F. Deschler, M. Saliba, H. Khandelwal, J. B. Patel, S. J. Elston, L. M. Herz, M. B. Johnston, A. P. Schenning, M. G. Debije, M. K. Riede, S. M. Morris, H. J. Snaith, *Nano Lett.* **2015**, *15*, 4935.
[19] W. A. P. M. Hendriks, L. Chang, C. I. Van Emmerik, J. Mu, M. De Goede, M. Dijkstra, S. M. Garcia-Blanco, *Adv. Phys.: X* **2021**, *6*, 1833753.
[20] G. M. Arumugam, C. Xu, S. K. Karunakaran, Z. Shi, F. Qin, C. Zhu, F. Chen, *J. Mater. Chem. C* **2018**, *6*, 12537.
[21] L. Protesescu, S. Yakunin, M. I. Bodnarchuk, F. Krieg, R. Caputo, C. H. Hendon, R. X. Yang, A. Walsh, M. V. Kovalenko, *Nano Lett.* **2015**, *15*, 3692.
[22] D. Qu, M. Archimi, A. Camposeo, D. Pisignano, E. Zussman, *ACS Nano* **2021**, *15*, 8753.
[23] a) G. Chilaya, in *Chirality in Liquid Crystals*, (Eds.: H.-S. Kitzerow, C. Bahr), Springer, New York, **2001**, Ch. 6, pp. 159–185; b) G. Meier, *Angew. Chem., Int. Ed.* **1980**, *19*, 656.
[24] Y. Xu, Z. Liu, L. Zhang, W. Qi, Q. Niu, W. Tan, W. Zeng, R. Xia, Y. Min, *Synth. Met.* **2022**, *283*, 116986.
[25] S. M. Jeong, K. Sonoyama, Y. Takanishi, K. Ishikawa, H. Takezoe, S. Nishimura, G. Suzaki, M. H. Song, *Appl. Phys. Lett.* **2006**, *89*, 241116.
[26] a) V. I. Kopp, B. Fan, H. K. M. Vithana, A. Z. Genack, *Opt. Lett.* **1998**, *23*, 1707; b) V. I. Kopp, A. Z. Genack, *Phys. Rev. Lett.* **2002**, *89*, 033901.
[27] a) N. Ganesh, W. Zhang, P. C. Mathias, E. Chow, J. A. N. T. Soares, V. Malyarchuk, A. D. Smith, B. T. Cunningham, *Nat. Nanotechnol.* **2007**, *2*, 515; b) A. Pokhriyal, M. Lu, V. Chaudhery, S. George, B. T. Cunningham, *Appl. Phys. Lett.* **2013**, *102*, 221114.
[28] Y. Xiong, Q. Huang, T. D. Canady, P. Barya, S. Liu, O. H. Arogundade, C. M. Race, C. Che, X. Wang, L. Zhou, X. Wang, M. Kohli, A. M. Smith, B. T. Cunningham, *Nat. Commun.* **2022**, *13*, 4647.
[29] a) Y.-H. Kim, S. Kim, A. Kakekhani, J. Park, J. Park, Y.-H. Lee, H. Xu, S. Nagane, R. B. Wexler, D.-H. Kim, S. H. Jo, L. Martínez-Sarti, P. Tan, A. Sadhanala, G.-S. Park, Y.-W. Kim, B. Hu, H. J. Bolink, S. Yoo, R. H. Friend, A. M. Rappe, T.-W. Lee, *Nat. Photonics* **2021**, *15*, 148; b) S. Kumar, T. Marcato, F. Krumeich, Y.-T. Li, Y.-C. Chiu, C.-J. Shih, *Nat. Commun.* **2022**, *13*, 2106.